Korean J. Chem. Eng., 39(8), 1981-1988 (2022)
DOI: 10.1007/s11814-022-1113-4

pISSN: 0256-1115
eISSN: 1975-7220

Sterically hindered amine-functionalized MCM-41 composite for efficient carbon dioxide capture

Fei Gao*, Cailin Ji*, Shougui Wang, Weiwen Wang*, Jipeng Dong*, Changqing Guo*, Yuwen Gao*, and Guanghui Chen*,†**

*Shandong Key Laboratory of Multiphase Fluid Reaction and Separation Engineering, College of Chemical Engineering, Qingdao University of Science and Technology, Qingdao, 266042, China
**Department of Chemical Engineering, Qingdao University of Science and Technology, Gaomi, 261500, China
(*Received 13 December 2021 • Revised 13 March 2022 • Accepted 15 March 2022*)

Abstract−A new adsorbent based on sterically hindered amine for efficient CO_2 capture was prepared. Mesoporous silicon MCM-41 was modified by sterically hindered amine AMPD (2-amino-2-methyl-1,3-propanediol) in different AMPD loadings by a facile solid-state self-assembly approach. The physicochemical properties of the MCM-41@AMPD composites were analyzed using XRD, BET, FT-IR and SEM, and the composites were investigated for the CO_2 capture performance, including CO_2 capture capacity, adsorption selectivity and cycling stability. Characterization analyses showed that the AMPD active components were successfully incorporated and well dispersed into the mesoporous silicon MCM-41 surfaces. Adsorption results suggest that the modification by the active ingredient AMPD can significantly improve the CO_2 capture performance. The MCM-41@AMPD material with an AMPD loading of 7 $mmol \cdot g^{-1}$ MCM-41 support exhibits a good CO_2 adsorption capacity and CO_2 adsorption selectivity, and shows excellent cycling stability. Furthermore, the isosteric heat of CO_2 adsorption on the MCM-41@AMPD-7 material was evaluated by the Clausius-Clapeyron equation, and the value was 34-78 $kJ \cdot mol^{-1}$.

Keywords: MCM-41@AMPD Composites, Carbon Dioxide, Adsorption, Selectivity, Reversibility

INTRODUCTION

Climate change caused by excessive greenhouse gases (GHGs) emissions has severely affected human survival and development. Among the GHGs, CO_2 is the major contributor to the greenhouse effect, and contributes higher than 60% of the GHGs [1]. It is mainly emitted from fossil fuel combustion for electric power generation and petrochemical production, especially the flue gases from thermal power plants, which accounts for nearly one-third of CO_2 emissions [2,3]. Although some emerging energy sources, including wind energy, solar energy and tidal energy, are available to mitigate carbon dioxide emissions, fossil fuels will remain the principal energy source to meet human survival needs in the foreseeable future [4]. Therefore, the urgent issue for alleviating climate change driven by CO_2 emission is to develop an effective adsorbent and/or technology for capturing CO_2 from the flue gases. The Chinese government promises to strive to achieve carbon peak before 2030, achieve carbon neutral before 2060 [5]. Carbon capture and storage (CCS) is recognized as the most efficient and realizable way to achieve carbon peak and carbon neutral, and the most energy-consuming procedure in CCS is CO_2 capture [6].

At present, various CO_2 capture technologies have been proposed, including cryogenic processes [7], chemical absorption [8], adsorption separation process [9], and membrane separation [10]. The absorption technology using aqueous monoethanolamine (MEA), methyldiethanolamine (MDEA), diethanolamine (DEA), etc. as absorbents has been considered as a relatively mature approach for capturing CO_2 in the industry, and has achieved a high CO_2 capture efficiency [11]. However, this method suffers from some significant challenges in the industrial application, including high equipment corrosion, solvent degradation, easy volatilization, foaming issues, especially the high energy consumption for the absorbent regeneration [12,13]. Adsorption by porous solid adsorbents is considered to be the most prospective substitute to replace the conventional absorption process by using amine solution because of its simple operation, high adsorption/desorption rate, free of equipment corrosion, and low regeneration cost [14,15]. The cornerstone of the adsorption process is the development of an efficient CO_2 adsorbent, which has an excellent CO_2 adsorption efficiency and CO_2 adsorption selectivity. At the same time, CO_2 adsorbent should be easy to recover and have good recycle capability. Up to now, numerous porous adsorbents have been reported for the CO_2 capture, such as basic metal oxides [16], metal organic frameworks (MOFs) [17], activated carbons [18], covalent organic frameworks (COFs) [19], zeolites [20], and mesostructured silicas materials [21]. Among these materials, MCM-41 silica with the highly ordered mesoporous has acquired wide attention owing to its outstanding features of large pore volume, greatly ordered and uniform porous structure, tunable pore sizes, high surface area, rich silanol groups, easy surface modification, high hydrothermal stability, and ease of synthesis [22,23]. MCM-41 has proven to be a promising material in the field of catalysis and adsorption separation, and is consid-

†To whom correspondence should be addressed.
E-mail: guanghui@qust.edu.cn
Copyright by The Korean Institute of Chemical Engineers.

ered an excellent substance for CO_2 adsorption. Nevertheless, pure MCM-41 displays low adsorption selectivity, sensitivity to the adsorption temperature, and poor water resistance owing to the physical interaction of MCM-41 with CO_2 by weak van der Waals force or electrostatic force [24]. Fortunately, the properties of MCM-41 can be easily chemically modified by incorporating basic groups to improve the CO_2 adsorption performance.

Amine functional groups modified solid adsorbents have received more and more attention for CO_2 adsorption, which combines the advantages of the easy regeneration of solid porous material and high CO_2 affinity of amine solution. The amine functional groups dispersed on the solid porous material provide abundant basic sites to react with acidic CO_2 gases reversibly, making the amine functionalized adsorbents show high CO_2 adsorption performance, high adsorption selectivity, good moisture tolerance and low energy consumption [25,26]. Therefore, amine groups modified MCM-41 is a promising material to prepare efficient CO_2 adsorbents, and has received widespread attention. Song and co-workers [27] first proposed an amine-modified MCM-41 solid adsorbent PEI/MCM-41 *via* impregnating PEI (polyethylenimine) into MCM-41, achieving a high CO_2 adsorption performance at 348 K. Since then, numerous amine-functionalized MCM-41 adsorbents [28-30] for CO_2 adsorption have been developed by impregnating or grafting various amines into MCM-41, such as monoethanolamine, diethanolamine, triethylenetetramine, and pentaethylenehexamine. After introducing amine functional groups, compared with original MCM-41, the CO_2 adsorption efficiency was significantly improved.

Currently, the majority of amine modification of MCM-41 has focused on the primary and secondary alkanolamines, reacting with CO_2 to form stable carbamates, therefore causing more time and energy consumption associated with the adsorbent regeneration [31]. Sterically hindered amines, typical 2-amino-2-methylpropanol (AMP) and 2-amino-2-methyl-1,3-propanediol (AMPD), tend to form unstable carbamates with CO_2 owing to the hindrance effect of the enormous group belonging to their amine groups, resulting in a less regeneration energy requirement [32]. In addition, sterically hindered amines have higher theoretical amine utilization efficiency and better degradation resistance in the CO_2 capture compared with non-hindered amines [33]. Sterically hindered amine solutions, such as AMP and AMPD have been widely researched for absorbing CO_2 [32,34]. Sterically hindered amine supported solid CO_2 adsorbents have rarely been reported. Generally, amine-modified solid adsorbents are mainly prepared by grafting or wet impregnation methods [13,35]. The preparation of amino-functionalized solid adsorbents using grafting approach, apart from the utilization of toxic and expensive organic solvents, always obtains lower amine loadings owing to the limited silanol content in the silicon material surfaces. Although sample preparation using wet impregnation method is considered to be superior to the grafting method in terms of easy synthesis and higher amine loadings, it requires an intensive solvent separation process, and the added amine active ingredient will not be completely introduced to the support pore channels due to the solvent effect, causing the waste of organic amines and the production of organic wastewater resulting from the unincorporated amines.

Herein, solid sterically hindered AMPD was assembled into mesostructured silicas MCM-41 to prepare the MCM-41@AMPD composites using a solid-state self-assembly method in an environment free of any water and organic solvent. The purpose of this work is to manufacture a new efficient CO_2 adsorbent by a facile fabrication method, and the amine active components will be completely introduced and well dispersed onto the surfaces of MCM-41. The synthesized MCM-41@AMPD materials with diverse AMPD loadings were analyzed by SEM, nitrogen adsorption and desorption test, FT-IR, and powder XRD. The CO_2 adsorption performance including the CO_2 adsorption capacity and the CO_2/N_2 adsorption selectivity for the synthesized MCM-41@AMPD composites were investigated, the reversibility and the isosteric adsorption heat of CO_2 were also determined.

EXPERIMENTAL

1. Materials

The commercial zeolite MCM-41 (H-type, All-silicon, Na_2O= 0.0008%) was purchased from Tianjin Nankai Catalyst Plant. 2-amino-2-methyl-1,3-propanediol (AMPD) was obtained from Shanghai Luoen Chemical Co., Ltd and used without any further purification. The gases of CO_2 (99.99%), He (99.999%) and N_2 (99.999%) were provided by Qingdao Dehai Gas Co., Ltd.

2. Preparation of Amine-functionalized MCM-41@AMPD

MCM-41@AMPD composites were prepared by a solid-state self-assembly approach. Appropriately, a specific amount of solid AMPD and MCM-41 powder was thoroughly ground and mixed, and then the mixed powder was activated in air at 383 K for 6 h to complete the spontaneous dispersion of the molten state AMPD active components into the MCM-41 pore channels through capillary action. According to the above process, the various composites with AMPD content of 3, 4, 5, 6, 7, 8 and 10 mmol·g^{-1} MCM-41were prepared. The synthesized samples are named as MCM-41@AMPD-*x*, where *x* is the content of AMPD per gram MCM-41 in mmol.

3. Sample Characterization

The structural characteristics of MCM-41@AMPD composites and MCM-41 were analyzed using the low-angle (2 theta=1-10°, 2°/min) and wide-angle (2 theta=10-80°, 10°/min) powder XRD data acquired by the Rigaku D-MAX 2500/PC diffractometer. The textural properties of the adsorbents were evaluated by nitrogen physical adsorption test by the Micromeritics ASAP 2460 Version 3.01 automatic physical adsorption instrument at 77 K. About 0.1 g of the adsorbent was degassed at 373 K under the vacuum for 4 h before each analysis. The total pore volumes of the materials were evaluated from total nitrogen adsorption under a relative pressure of p/p_0=0.95, and the conventional Brunauer-Emmett-Teller (BET) method was used to estimate the specific surface areas. The change of functional group in the adsorbents was checked by FT-IR spectra collected using a Thermo-Scientific Nicolet iS10 FT-IR instrument from 400 to 4,000 cm^{-1}. In addition, the morphology change of the sample before and after modification was identified by a Sigma-500 scanning electron microscope (SEM) instrument.

4. Adsorption Isotherm Tests

A static adsorption device was applied to perform the CO_2 and N_2 adsorption isotherm measurements, and the operation and cal-

culation procedures were sufficiently presented in our prior work [36]. The adsorption was measured in the pressure range of 0-500 kPa at a given temperature kept by the circulating water bath. Before each test, the adsorbents were processed at 353 K for 4 h under the vacuum.

5. Adsorption Theories

5-1. Adsorption Isotherm Modeling

In this work, in order to calculate the isosteric heat of CO_2 adsorption and the CO_2/N_2 adsorption selectivity on the prepared adsorbents, the CO_2 and N_2 adsorption points were correlated using Sips adsorption isotherm model, and this model is expressed as [37]:

$$q = q_m \frac{bp^{1/n}}{1+bp^{1/n}} \quad (1)$$

where q represents the adsorption capacity ($mmol \cdot g^{-1}$) at a adsorption equilibrium pressure p (kPa), q_m represents the amount adsorbed at saturation ($mmol \cdot g^{-1}$), b represents the Sips correlative coefficient (kPa^{-1}), n expresses the adsorbent heterogeneity.

The mean deviation (D) was calculated to assess the accuracy of the fit of the Sips model to the adsorption data according to the following equation:

$$D\ (\%) = \frac{100}{N}\sum_{i=1}^{N}\left|\frac{q_i^{exp} - q_i^{cal}}{q_i^{exp}}\right| \quad (2)$$

where N is the number of adsorption data points, q^{exp} is the experimental adsorption capacity, and q^{cal} is the adsorption capacity calculated from the fitted Sips model.

5-2. Adsorption Selectivity

CO_2 selectivity is one of the most important indexes to evaluate the selective separation CO_2 capacity of adsorbents for the gas mixtures. Ideal adsorption solution theory (IAST) [38] is the most common theory for predicting the multi-component adsorption from single component adsorption isotherm. The adsorption selectivity of CO_2/N_2 (S_{CO_2/N_2}) for a mixed gas of CO_2 and N_2 was estimated on the basis of the following equation [39]:

$$S_{CO_2/N_2} = \frac{x_{CO_2}/x_{N_2}}{y_{CO_2}/y_{N_2}} \quad (3)$$

where x refers to the mole fraction of CO_2 and N_2 in the adsorbed phase, y refers to the mole fraction in the bulk phase.

5-3. Adsorption Isosteric Heat

According to the fitted adsorption isotherms at different temperatures from the measured adsorption data, the Clausius-Clapeyron equation was applied to determine the isosteric heat of CO_2 adsorption [40]:

$$Q_{st} = RT^2\left(\frac{\partial \ln p}{\partial T}\right)_{q_a} \quad (4)$$

where Q_{st} is the isosteric heat of adsorption ($kJ \cdot mol^{-1}$), R is the ideal gas constant ($J \cdot mol^{-1} \cdot K^{-1}$), T is the absolute temperature (K), and q_a is a given CO_2 loading ($mmol \cdot g^{-1}$).

RESULTS AND DISCUSSION

1. Characterization of Composite

Fig. 1 illustrates the X-ray diffraction patterns in low angle and wide angle of pure AMPD, pristine MCM-41 and MCM-41@AMPD-7. In Fig. 1(a), the pristine MCM-41 sample shows a sharp diffraction peak at 2θ=2.3° and two weak peaks at 2θ=3.9° and 4.5°, which are assigned to (100), (110) and (200) planes of the representative feature of MCM-41 framework, indicative of the presence of hexagonal mesopores with regular arrangement [22]. After modification with AMPD, the diffraction intensity of (100) plane of MCM-41@AMPD-7 was significantly reduced, whereas the (110) and (200) diffraction peaks disappeared, attributed to the effect of pore filling of MCM-41 by AMPD, resulting in a reduction in scattering contrast due to the contrast matching between the siliceous framework in MCM-41 and introduced AMPD molecules [4]. Additionally, the (100) diffraction peak slightly shifted towards a higher angle for the MCM-41@AMPD-7 sample, indicating that the AMPD species were effectively incorporated into the MCM-41 support pore channels [41]. From Fig. 1(b), the pure AMPD was detected by high angle XRD; however, no AMPD diffraction peaks were detected in the MCM-41@AMPD-7 sample, indicating that, during the activation at 383 K, the molten state AMPD were highly dispersed into the MCM-41support pore channels through

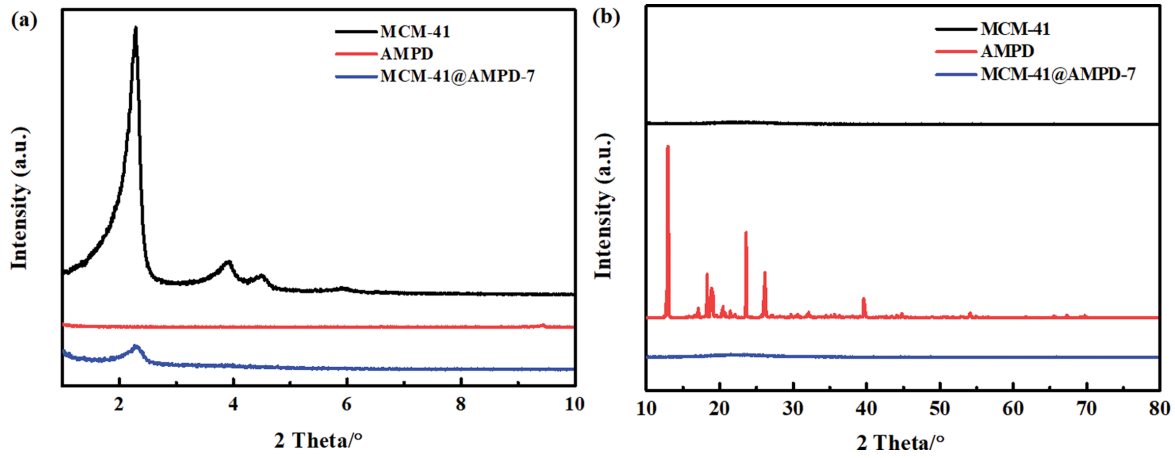


Fig. 1. Low angle XRD pattern (a) and wide angle XRD pattern (b) of MCM-41, AMPD and MCM-41@AMPD-7.

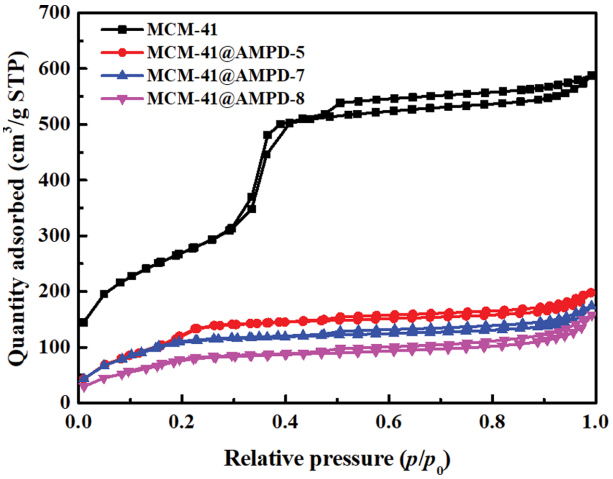


Fig. 2. N_2 adsorption and desorption isotherms of MCM-41 and MCM-41@AMPD composites with different AMPD loading at 77 K.

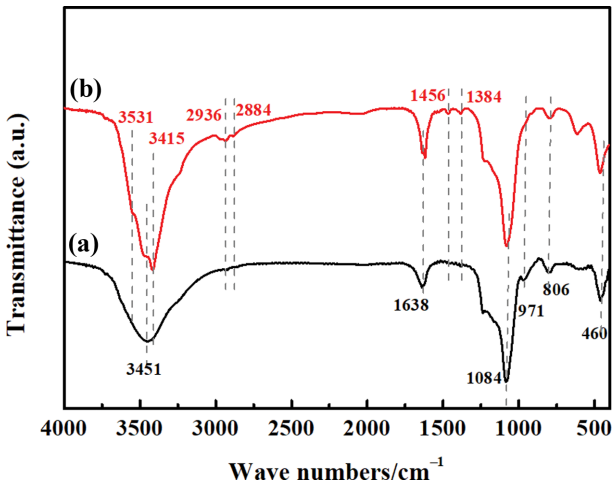


Fig. 3. FT-IR spectra of MCM-41 (a), MCM-41@AMPD-7 (b).

Table 1. Textural properties of MCM-41 and MCM-41@AMPD composites

Sample	BET surface area ($m^2 \cdot g^{-1}$)	Total pore volume ($cm^3 \cdot g^{-1}$)
MCM-41	978	0.866
MCM-4 1@AMPD-5	500	0.269
MCM-4 1@AMPD-7	390	0.227
MCM-4 1@AMPD-8	297	0.192

the capillary action or converted to amorphous species.

Fig. 2 displays the N_2 adsorption and desorption isotherms of MCM-41@AMPD composites with different AMPD content and the pristine MCM-41, and Table 1 lists data on the textural properties of these adsorbents, including the specific surface areas and total pore volumes. As shown in Fig. 2, the parent MCM-41 displays a typical type IV adsorption isotherm with a H4 hysteresis loop based on the IUPAC classification, characterizing the mesoporous property of MCM-41 [35,42]. The MCM-41 adsorption isotherm shows a dramatic increase in N_2 adsorption amount at the relative pressure of p/p_0 from 0.30 to 0.41 owing to the nitrogen capillary condensation in the mesopores, indicating the signature of uniform mesostructure of the sample [4,35,43]. After the modification by AMPD, the hysteresis loop could still be observed in the isotherms of MCM-41@AMPD composites. For the MCM-41@AMPD composites, the total pore volumes and specific surface areas decrease after the functionalization with AMPD, which is caused by the introduction of functional groups occupying part of the pore space of the MCM-41 support. The above results indicate that functional AMPD components are successfully incorporated into the mesopores of MCM-41.

The change of surface functional groups was identified using FT-IR spectroscopy. The MCM-41@AMPD-7 and pristine MCM-41 FT-IR spectra are presented in Fig. 3. In the pristine MCM-41 FT-IR spectrum, the peaks at 3,451 and 1,638 cm^{-1} are related to the -OH groups stretching and bending vibrations of the silanols and physically adsorbed water on MCM-41 surface [1]. The bands at 460, 806 and 1,084 cm^{-1} are assigned to the bending, symmetric stretching and asymmetric stretching vibrations of Si-O-Si bonds, and the band at 971 cm^{-1} is attributed the Si-O stretching vibration of Si-OH in MCM-41 framework [44]. After functionalization with AMPD, all the vibration peaks of MCM-41 can still be observed in the MCM-41@AMPD composite spectrum, indicating that the composites retain the MCM-41 framework structure. Apparently, after introducing AMPD, new bands around 3,415 and 3,531 cm^{-1} are observed, which represent the -NH_2 group symmetric and asymmetric stretching vibrations [45]. The bands of 2,936 and 2,884 cm^{-1} representing C-H asymmetric and symmetric stretching vibrations can be observed in Fig. 3 [12]. In addition, the bands at 1,456 and 1,384 cm^{-1} correspond to the C-H bending vibration in AMPD molecules [45]. The results indicate that the functional amino components are effectively introduced into MCM-41. Moreover, compared with MCM-41, the stretching vibration peak around 3,451 cm^{-1} of silanols in MCM-41 framework became narrower and sharper, and the position of the Si-OH and Si-O-Si bond vibration peaks shifted. This may be caused by the interaction of the Si-OH groups in MCM-41 framework with the -NH_2 groups in AMPD molecules, forming the hydrogen bonds, which is conducive to the stability of the amine active component supported on the support [46].

Fig. 4 presents the SEM images of the MCM-41@AMPD-7 composite and the pristine MCM-41 to characterize the morphology change of the sample before and after the amine modification. In the pristine MCM-41 SEM images (Fig. 4(a) and (b)), some irregular particles with the sizes of about 100-300 nm are observed, and abundant pores are observed on the particle surfaces, leading to the outstanding structural property of the MCM-41 support with high specific surfaces and large pore volumes, which facilitate the AMPD functional components loading. In the SEM images of MCM-41@AMPD-7 composite (Fig. 4(c) and (d)), it can be seen that the morphology of the composite has no significant change after the AMPD modification, indicating well dispersed AMPD active components in the MCM-41 support pore channels rather than the aggregation on the support surfaces. This result is consis-

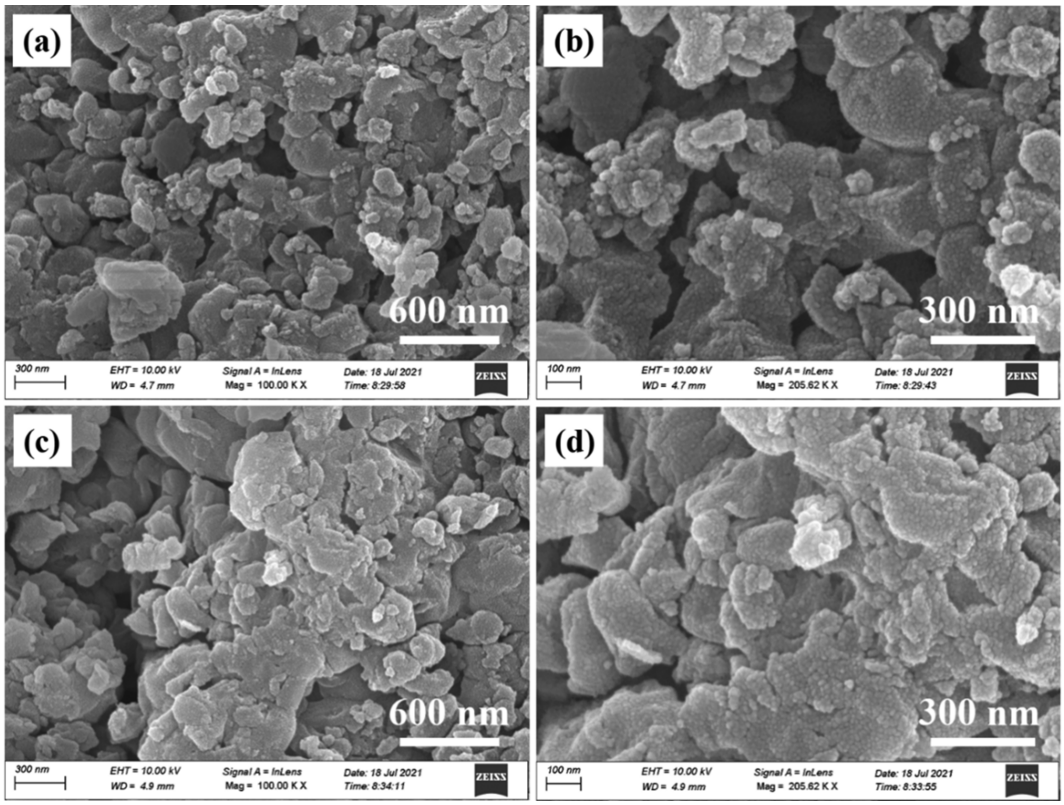


Fig. 4. SEM images of MCM-41 (a), (b) and MCM-41@AMPD-7 composite (c), (d) at different magnification.

tent with the result of XRD analysis.

2. Adsorption Performance of CO_2 on MCM-41@AMPD Composites

Fig. 5 illustrates the CO_2 adsorption isotherms of pure AMPD, support and MCM-41@AMPD composites with various AMPD loadings at 303 K. As shown in Fig. 5, the pure AMPD displays a low CO_2 adsorption capacity because the low surface area and pore volume of the pure AMPD sample prevented the diffusion of

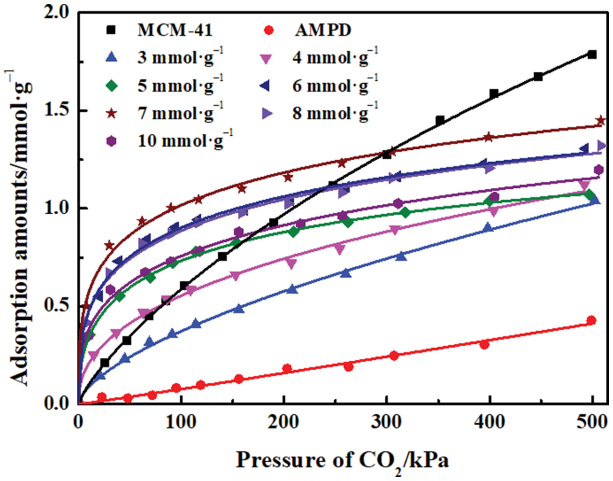


Fig. 5. CO_2 adsorption isotherms on pure AMPD, MCM-41 support and the MCM-41@AMPD adsorbents with various AMPD contents at 303 K.

CO_2 molecules into the sample. The support of MCM-41 exhibits a higher CO_2 adsorption capacity of 1.78 mmol·g^{-1} at 500 kPa because of its large pore volume and high specific surface area, caused by the physical interaction *via* van der Waals force or electrostatic force between CO_2 and MCM-41. The adsorption capacity of CO_2 on MCM-41@AMPD composites at low adsorption pressure was significantly enhanced compared with that of the MCM-41 support, revealing that the introduced AMPD was significantly effective in enhancing the CO_2 adsorption capacity. In addition, the CO_2 adsorption amount on the MCM-41@AMPD composites gradually increases when increasing the AMPD content to 7 mmol·g^{-1} MCM-41 support. This behavior is caused by the fact that AMPD occupies part of the pore volume and surface area of the MCM-41 support, leading to that the chemisorption of -NH_2 groups with CO_2 molecules gradually replace the physisorption for CO_2 on the adsorbents as the loading of AMPD increasing. When further increasing AMPD loadings to 10 mmol·g^{-1} MCM-41 support, the CO_2 adsorption capacity drops sharply, which may be ascribed to the excessive AMPD species accumulation on the surfaces of the composites, causing effective active site reduction and clogging of pores. Therefore, the appropriate loading of AMPD on the used MCM-41 support is 7 mmol·g^{-1}. The prepared MCM-41@AMPD-7 composite achieves a higher CO_2 adsorption amount of 1.45 mmol·g^{-1} at 500 kPa, and the adsorption amount of CO_2 on MCM-41@AMPD-7 sample is almost twice that of MCM-41 support at a low pressure of 100 kPa.

The content of N_2 in the coal-fired flue gases is ~85%, which makes it become the main competitive gas hindering the CO_2 cap-

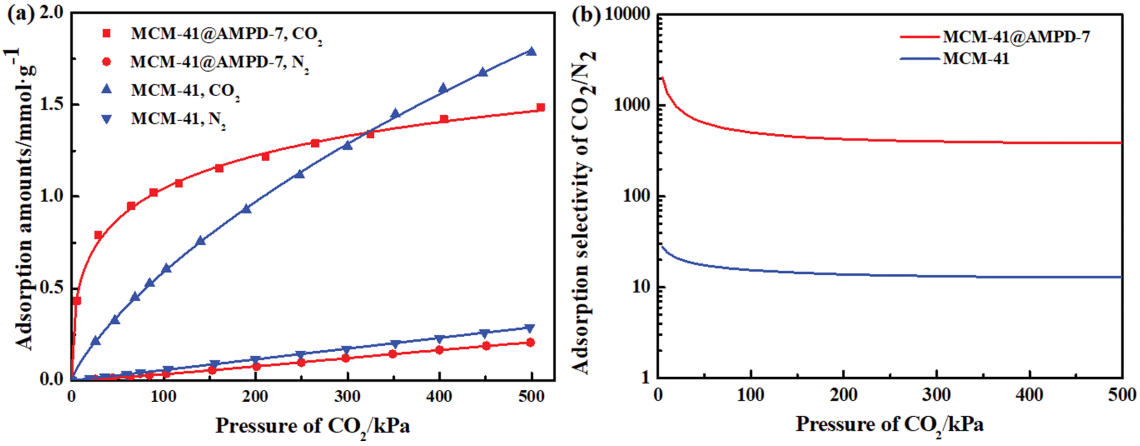


Fig. 6. CO_2 and N_2 adsorption isotherms of on MCM-41@AMPD-7 and MCM-41 at 303 K (a) and CO_2/N_2 adsorption selectivity for the CO_2/N_2 (15 : 85) mixture (b).

Table 2. Sips fitting parameters with mean deviations for CO_2 and N_2 adsorption on MCM-41@AMPD-7

Parameters	q_m (mmol·g^{-1})	b×10^3 (kPa^{-1})	n	D (%)
MCM-41@AMPD				
CO_2 (303 K)	2.62	104	2.48	1.94
CO_2 (313 K)	2.31	64.4	1.98	2.56
CO_2 (323 K)	2.12	34.8	1.63	2.03
CO_2 (333 K)	1.98	17.2	1.40	1.63
N_2 (303 K)	1.00	0.104	0.79	3.10
MCM-41				
CO_2 (303 K)	4.58	2.27	1.10	2.39
N_2 (303 K)	1.51	0.204	0.88	2.66

ture [47]. Therefore, the CO_2/N_2 adsorption selectivity on the fabricated MCM-41@AMPD-7 toward the CO_2/N_2 binary mixture (15/85) was determined using the IAST based on the fitted pure CO_2 and N_2 adsorption isotherms (see Fig. 6(a)), and compared with the adsorption selectivity of the pristine MCM-41. The pure component adsorption data were well correlated with the Sips isotherm model and the correlated model information is shown in Table 2. As shown in Fig. 6(a), the CO_2 adsorption performance of MCM-41@AMPD-7 is significantly better than the N_2 adsorption performance and the N_2 adsorption capacity decreases when introducing the amine groups on MCM-41, due to the reduction of surface area and pore volume of the composite. Fig. 6(b) presents the IAST adsorption selectivity of CO_2/N_2 on MCM-41@AMPD-7 and MCM-41 as a function of pressure. The adsorption selectivity of CO_2/N_2 values decrease rapidly with the adsorption pressure at low pressures and gradually reach a constant at higher pressures, which may be due to the more CO_2 active sites at low pressures, confirmed by the isosteric heat of adsorption (see Fig. 8 below). Moreover, the adsorption selectivity is comparatively higher for MCM-41@AMPD-7 composite than pristine MCM-41 sample in the whole experimental pressure range. At 100 kPa, the pristine MCM-41 sample suggests a CO_2/N_2 adsorption selectivity of 15, while MCM-41@AMPD-7 composite shows adsorption selectivity of 520, almost 35 times that the MCM-41 support. This greater CO_2/N_2 selectivity could be explained by the fact that the introduced Lewis base amine functional groups with good affinity for Lewis acid CO_2 resulted in high CO_2 adsorption and high selectivity over N_2. The results show that the formed MCM-41@AMPD-7 composite would be a promising candidate for the CO_2/N_2 separation.

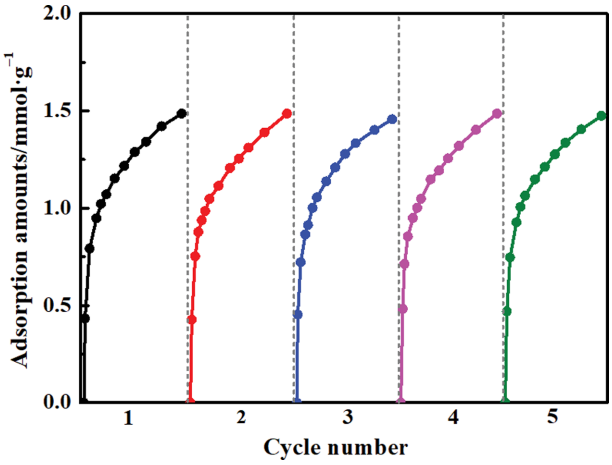


Fig. 7. CO_2 cyclic adsorption capacity on MCM-41@AMPD-7 with adsorption at 303 K and desorption at 353 K.

Apart from the CO_2 adsorption capacity and CO_2/N_2 adsorption selectivity, the cycle stability of CO_2 adsorbents is also important for their practical industrial application. Therefore, to evaluate the cyclic stability for CO_2, consecutive five CO_2 adsorption and desorption cycles on the MCM-41@AMPD-7 adsorbent were performed. The adsorption was conducted at 303 K, and the adsorbent was regenerated in situ under vacuum at 353 K. Fig. 7 illustrates the cyclic adsorption isotherms for CO_2 in the five cyclic tests. The result shows that there is no significant change in the adsorption capacity for CO_2 in the five cycles, indicating that the adsorbents possess good recyclability. Note that the MCM-41@AMPD adsorbent after adsorbing CO_2 can be regenerated at a relatively low temperature of 353 K, and this mild regeneration condition is attributed to the use of hindered amines as active sites, providing an appro-

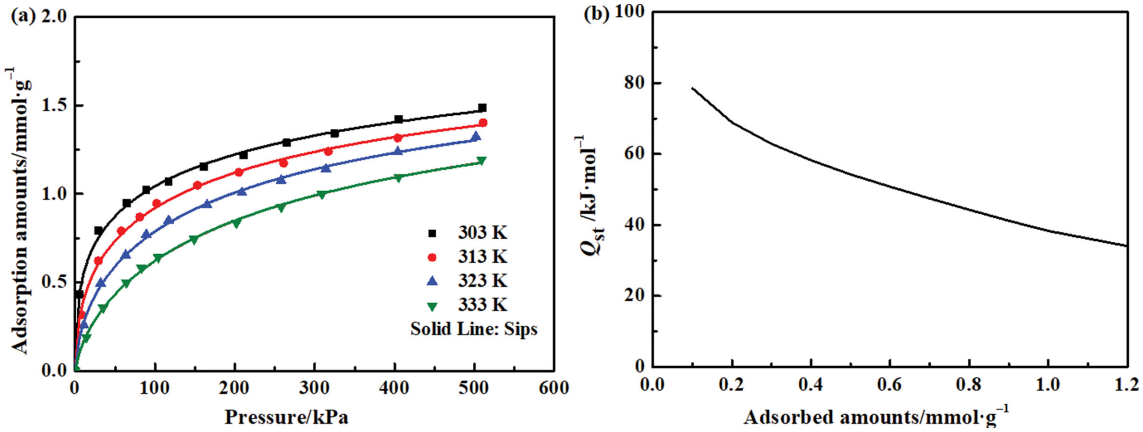


Fig. 8. CO_2 adsorption isotherms at various temperatures (a) and adsorption isosteric heats for CO_2 on MCM-41@AMPD-7 as a function of CO_2 loading (b).

priate interaction strength of CO_2 with adsorbent.

The crucial parameter for revealing the strength of adsorbate-adsorbent interaction and designing the gas separation adsorber is the isosteric heat of adsorption. The isosteric heat of CO_2 adsorption on the MCM-41@AMPD-7 adsorbent was determined according to Eq. (3) according to the fitted CO_2 adsorption isotherms at the various temperatures, as shown in Fig. 8(a). Table 2 lists the fitted model coefficients with mean deviations, and the calculated adsorption heats results are presented in Fig. 8(b). From Table 2, the adsorption data are well fitted by the Sips model. From Fig. 8(a), the CO_2 adsorption capacity on MCM-41@AMPD-7 sample shows a downward trend with increasing the adsorption temperature, indicating that there is an exothermic process of the CO_2 adsorption on MCM-41@AMPD-7 composites. From Fig. 8(b), the isosteric heats of CO_2 adsorption on MCM-41@AMPD-7 are in the range of 78-34 kJ·mol^{-1} at a CO_2 coverage of 0.1-1.2 mmol·g^{-1}. The values over the whole CO_2 cover are higher than that of a weak physisorption process (<20 kJ·mol^{-1}) [48], demonstrating that the CO_2 adsorption on MCM-41@AMPD adsorbent is a chemisorption process due to the high CO_2 affinity of -NH_2 groups. Generally, the heats of adsorption for the strong chemisorption range from 60 to 90 kJ·mol^{-1} [49]. It was proposed that the amount of amino active sites in the adsorbent has an effect on the heat of adsorption, and the higher amount of amino groups will increase the adsorption heat [37,49]. The higher initial isosteric heat of CO_2 adsorption on MCM-41@AMPD-7 adsorbent may be owing to the large number of readily available amine sites in the composite at low CO_2 loading, resulting in a fast and strong interaction between the MCM-41@AMPD-7 composite and CO_2 molecules. With increasing CO_2 loading, the decline of the adsorption heat may be attributed to the continuous active sites occupation, resulting in a lack of available active sites. This relatively low isosteric heat of adsorption makes the composite require lower energy for regenerating the adsorbent.

CONCLUSIONS

Sterically hindered amine AMPD supported MCM-41 adsorbents (MCM-41@AMPD) with various AMPD loading were successfully obtained for the effective adsorption of CO_2 by a facile and feasible method. No organic solvents and additives were used in the preparation process, and amine active components AMPD were completely introduced into the MCM-41. During the activation process at 383 K, the AMPD species were highly dispersed into the MCM-41 mesoporous structure. After the amine functionalization, the composites still maintained a mesoporous structure. The optimized adsorbent MCM-41@AMPD has an AMPD loading of 7 mmol·g^{-1} MCM-41, obtaining a significant improvement in CO_2 capture capability compared with MCM-41. MCM-41@AMPD-7 composite shows a high CO_2/N_2 adsorption selectivity of 520 at 100 kPa, which is almost 35 times that of the MCM-41 support. After five cycles of CO_2 adsorption and desorption test, the CO_2 adsorption capacity of MCM-41@AMPD-7 remained basically unchanged. The relatively low isosteric heat of CO_2 adsorption of 34-78 kJ·mol^{-1} on MCM-41@AMPD-7 shows the composite need a lower energy requirement for regenerating the adsorbent. The excellent adsorption performance makes the MCM-41@AMPD composite a potential candidate for separating CO_2 from gas mixtures, and could achieve mild operating conditions.

ACKNOWLEDGEMENTS

This work was funded by Natural Science Foundation of Shandong Province with Grant No. ZR2021MB135, and Qingdao Science and Technology Plan Application Foundation Research Project with Grant No. 19-6-2-28-cg.

CONFLICT OF INTEREST STATEMENT

There are no conflicts to declare.

REFERENCES

1. X. Zhang, Y. Huang, J. Yang, H. Gao, Y. Huang, X. Luo, Z. Liang and P. Tontiwachwuthikul, *Chem. Eng. J.*, **383**, 123077 (2020).
2. Y.-J. Heo, D. B. Seong and S.-J. Park, *J. CO_2 Util.*, **34**, 472 (2019).
3. S. Shang, Z. Tao, C. Yang, A. Hanif, L. Li, D. C. W. Tsang, Q. Gu and J. Shang, *Chem. Eng. J.*, **393**, 124666 (2020).

4. S. Ahmed, A. Ramli and S. Yusup, *Fuel Process. Technol.*, **167**, 622 (2017).
5. X. Shi, Y. Zheng, Y. Lei, W. Xue, G. Yan, X. Liu, B. Cai, D. Tong and J. Wang, *Sci. Total Environ.*, **795**, 148784 (2021).
6. R. S. Haszeldine, *Science*, **325**, 1647 (2009).
7. C. Song, Q. Liu, S. Deng, H. Li and Y. Kitamura, *Renew. Sust. Energ. Rev.*, **101**, 265 (2019).
8. E. O. Agbonghae, K. J. Hughes, D. B. Ingham, L. Ma and M. Pourkashanian, *Ind. Eng. Chem. Res.*, **53**, 14815 (2014).
9. N. Hedin, L. Andersson, L. Bergström and J. Yan, *Appl. Energy*, **104**, 418 (2013).
10. A. Brunetti, E. Drioli, Y. M. Lee and G. Barbieri, *J. Membr. Sci.*, **454**, 305 (2014).
11. M. Garcia, H. K. Knuutila, U. E. Aronu and S. Gu, *Int. J. Greenh. Gas Control*, **78**, 286 (2018).
12. C. Zhou, S. Yu, K. Ma, B. Liang, S. Tang, C. Liu and H. Yue, *Chem. Eng. J.*, **413**, 127675 (2021).
13. M. G. Yıldız, T. Davran-Candan, M. Erdem Günayc and R. Yıldırım, *J. CO_2 Util.*, **31**, 27 (2019).
14. A. S. Bhown and B. C. Freeman, *Environ. Sci. Technol.*, **45**, 8624 (2011).
15. R. Dey and A. Samanta , *Korean J. Chem. Eng.*, **37**, 1951 (2020).
16. K. K. Han, Y. Zhou, Y. Chun and J. H. Zhu, *J. Hazard. Mater.*, **203**, 341 (2012).
17. K. Pirzadeh, K. Esfandiari, A. A. Ghoreyshi and M. Rahimnejad, *Korean J. Chem. Eng.*, **37**, 513 (2020).
18. H. Burri, R. Anjum, R. B. Gurram, H. Mitta, S. Mutyala and M. Jonnalagadda, *Korean J. Chem. Eng.*, **36**(9), 1482 (2019).
19. N. Huang, X. Chen, R. Krishna and D. Jiang, *Angew. Chem. Int. Ed.*, **54**, 2986 (2015).
20. A. A. Dabbawala, I. Ismail, B. V. Vaithilingam, K. Polychronopoulou, G. Singaravel, S. Morin, M. Berthod and Y. A. Wahedi, *Micropor. Mesopor. Mater.*, **303**, 110261 (2020).
21. R. Sanz, G. Calleja, A. Arencibia and E. S. Sanz-Pérez, *Micropor. Mesopor. Mater.*, **209**, 165 (2015).
22. S. Cheng, Y. Liu and G. Qi, *Chem. Eng. J.*, **400**, 125946 (2020).
23. H. P. Lin, Y. R. Cheng, C. R. Lin, F. Y. Li, C. L. Chen, S. T. Wong, S. Cheng, S. B. Liu, B. Z. Wan and C. Y. Mou, *J. Chin. Chem. Soc.*, **46**, 495 (1999).
24. S. Mukherjee, Akshay and A. N. Samanta, *Adv. Powder Technol.*, **30**, 3231 (2019).
25. X. Hu, L. Liu, X. Luo, G. Xiao, E. Shiko, R. Zhang, X. Fan, Y. Zhou, Y. Liu, Z. Zeng and C. Li, *Appl. Energ.*, **260**, 114244 (2020).
26. P. Zhao, Y. Yin, W. Cheng, X. Xu, D. Yang and W. Yuan, *J. CO_2 Util.*, **50**, 101612 (2021).
27. X. Xu, C. Song, J. M. Andresen, B. G. Miller and A. W. Scaroni, *Energ. Fuel*, **16**, 1463 (2002).
28. R. S. Franchi, P. J. E. Harlick and A. Sayari, *Ind. Eng. Chem. Res.*, **44**, 8007 (2005).
29. M. B. Yue, L. B. Sun, Y. Cao, Y. Wang, Z. J. Wang and J. H. Zhu, *Chem. Eur. J.*, **14**, 3442 (2008).
30. K. S. N. Kamarudin and N. Alias, *Fuel Process. Technol.*, **106**, 332 (2013).
31. F. Bougie and M. C. Iliuta, *J. Chem. Eng. Data*, **57**, 635 (2012).
32. F. Bougie and M. C. Iliuta, *Chem. Eng. Sci.*, **65**, 4746 (2010).
33. J. J. Lee, C. Sievers and C. W. Jones, *Ind. Eng. Chem. Res.*, **58**, 22551 (2019).
34. H. Esmaeili and B. Roozbehani, *Int. J. Greenh. Gas Con.*, **30**, 212 (2014).
35. X. Wang, L. Chen and Q. Guo, *Chem. Eng. J.*, **260**, 573 (2015).
36. F. Gao, Y. Wang and S. Wang, *Chem. Eng. J.*, **290**, 418 (2016).
37. Y. Hosseini, M. Najafi, S. Khalili, M. Jahanshahi and M. Peyravi, *Mater. Chem. Phys.*, **270**, 124788 (2021).
38. A. L. Myers and J. M. Prausnitz, *AIChE J.*, **11**(1), 121 (1965).
39. S. Khalili and M. Jahanshahi, *Korean J. Chem. Eng.*, **38**(4), 862 (2021).
40. R. Melouki, A. Ouadah and P. L. Llewellyn, *J. CO_2 Util.*, **42**, 101292 (2020).
41. M. U. T. Le, S.-Y. Lee and S.-J. Park, *Int. J. Hydrogen Energy*, **39**, 12340 (2014).
42. K. S. W. Sing, D. H. Everett, R. A. W. Haul, L. Moscou, R. A. Pierotti, J. Rouquerol and T. Siemieniewska, *Pure Appl. Chem.*, **57**, 603 (1985).
43. E. Vunain, N. N. Opembe, K. Jalama, A. K. Mishra and R. Meijboom, *J. Therm. Anal. Calorim.*, **115**, 1487 (2014).
44. S. Sharma, U. P. Singh and A. P. Singh, *Polyhedron*, **199**, 115102 (2021).
45. T. S. Renuga Devi, J. Sharmi kumar and G. R. Ramkumaar, *Acta A*, **133**, 214 (2014).
46. G. Zhang, P. Zhao, L. Hao and Y. Xu, *J. CO_2 Util.*, **24**, 22 (2018).
47. L.-B. Sun, A.-G. Li, X.-D. Liu, X.-Q. Liu, D. Feng, W. Lu, D. Yuan and H.-C. Zhou, *J. Mater. Chem. A*, **3**, 3252 (2015).
48. L. Liu, G. Zou, B. Yang, X. Luo and S. Xu, *ACS Appl. Nano Mater.*, **1**, 4695 (2018).
49. T. Watabe and K. Yogo, *Sep. Purif. Technol.*, **120**, 20 (2013).